CHAPTER 2

Distribution of isolated volcanoes on the flanks of the East Pacific Rise, 15.3˚S-20˚S

Abstract. Volcanic constructions, not associated with seamount (or volcano) chains, are abundant on the flanks of the East Pacific Rise (EPR) but are rare along the axial high. The distribution of isolated volcanoes, based on multibeam bathymetric maps, is approximately symmetric about the EPR axis. This symmetry contrasts with the asymmetries in the distribution of volcano chains (more abundant on the west flank), the seafloor subsidence rates (slower on the west flank), and the distribution of plate-motion-parallel gravity lineaments (more prominent on the west flank). Most of the isolated volcanoes complete their growth within ~14 km of the axis on crust younger than 0.2 Ma, while seamount chain volcanoes continue to be active on older crust. Volcanic edifices within 6 km of the ridge axis are primarily found adjacent to axial discontinuities, suggesting a more sporadic magma supply and stronger lithosphere able to support volcanic constructions near axial discontinuities. The volume of isolated near-axis volcanoes correlates with ridge axis cross-sectional area, suggesting a link between the magma budget of the ridge and the eruption of near-axis volcanoes. Within the study area, off-axis volcanic edifices cover at least 6% of the seafloor and contribute more than 0.2% to the volume of the crust. The inferred width of the zone where isolated volcanoes initially form increases with spreading rate for the Mid-Atlantic Ridge (<4 km), northern EPR (<20 km), and southern EPR (<28 km), so that isolated volcanoes form primarily on lithosphere younger than 0.2 Ma (< 4-6 km brittle thickness), independent of spreading rate. This suggests some form of lithospheric control on the eruption of isolated off-axis volcanoes due to brittle thickness, increased normal stresses across cracks impeding dike injection, or thermal stresses within the newly forming lithosphere.

1. Introduction

Off-axis volcanoes created near fast-spreading mid-ocean ridges provide insight about the processes occurring in the early stages of oceanic lithosphere formation. The distribution of the chains of large volcanoes (> 200 m high) has been documented along the southern East Pacific Rise (EPR) in a variety of studies [e.g., *Batiza*, 1982; *Smith and Jordan*, 1988; *Bemis and Smith*, 1993; *Scheirer and Macdonald*, 1995; *Shen et al.*, 1995; *Scheirer et al.*, 1996b; *Rappaport et al.*, 1997]. Smaller

volcanoes have not been well documented previously, as their size makes them difficult to detect in abyssal hill terrain without high-resolution, full-coverage multibeam bathymetry which has only recently become available [*Scheirer et al.*, 1996a,c]. Also, recent advances in understanding the structure of abyssal hills [*Macdonald et al.*, 1996] make it possible to distinguish small volcanic constructions from the seafloor fabric of abyssal hills. At slow to intermediate spreading rates, volcanic edifices are built on the ridge axis itself [e.g., *Smith and Cann*, 1992; *Kleinrock et al.*, 1994; *Magde and Smith*, 1995; *Smith et al.*, 1995]. In contrast, the only previous study of near-axis volcanoes along a fast spreading ridge, EPR at 9˚-10˚N, concluded that small isolated volcanoes form outside the neovolcanic zone, 5-10 km from the ridge axis, on crustal ages of 0.1-0.2 Ma [*Alexander and Macdonald*, 1996].

The EPR from 15˚S to 20˚S has been the focus of numerous studies, including bathymetric mapping, seismic surveys, the MELT experiment, petrologic investigations, and deep-submergence vehicle operations on the ridge axis (Figure 1) [*Forsyth et al.*, 1998; *MELT Seismic Team*, 1998; *Scheirer et al.*, 1998]. This study focuses on near-axis volcanoes, cataloging all the topographic highs with at least 50 m relief and a quasi-circular base, on crust out to magnetic anomaly 2 (~1.9 Ma) along 520 km of the EPR (Figure 2). We map the distribution of near-axis isolated volcanoes along and across the ridge axis and then place these observations in the context of genetic models for off-axis volcanism near fast-spreading ridges. Volcanoes under 200 m high have not been included in previous studies of the off-axis volcanism along the southern EPR (SEPR), and many of the volcanoes east of the ridge were mapped in 1996 [*Scheirer et al.*, 1998] after the initial study of the Rano Rahi Seamount Field [*Scheirer et al.*, 1996b].

2. Geological Framework of the Study Area: Overview of the EPR From 15˚ to 20˚S

Located between the Easter Microplate and the Garrett Fracture Zone, the EPR within the study area is an ultra-fast spreading ridge (Figure 1). Since 1 Ma, the Pacific plate has been spreading slightly faster than the Nazca plate north of 17˚15’S, at a half-rate of 75 mm/yr versus 65 mm/yr. The asymmetry reverses just south of 17˚15’S, so that the Nazca Plate is spreading eastward at a half-rate of 80 mm/yr, roughly 20 mm/yr faster than the Pacific plate half-rate [*Cormier et al.*, 1996; D. Wilson, personal communication, 1997]. Bathymetric mapping reveals that the seafloor on the Pacific plate subsides at a slower rate than predicted by the global average of lithospheric cooling with crustal age,

implying hotter mantle and thinner lithosphere on the west flank [*Cochran*, 1986; *Scheirer et al.*, 1998].

Seven small overlapping spreading centers (OSCs) are located within the study area at approximately 15˚55'S, 16˚30'S, 17˚56'S, 18˚22'S, 18˚37'S, 19˚05'S, and 19˚50'S [*Lonsdale*, 1989; *Scheirer et al.*, 1996a](Figure 2). These OSCs are all left-stepping offsets whose propagation history explains most of the spreading asymmetry [*Cormier and Macdonald*, 1994; *Cormier et al.*, 1996]. The 15˚55'S OSC has remained relatively stationary, the 16˚30'S OSC has migrated northward, and the other OSCs have been rapidly migrating south [*Cormier et al.*, 1996]. The presence of a long-lived axial magma chamber (AMC) has been inferred from the continuity of a midcrustal seismic reflector under the ridge through most of this region, except near OSCs [*Detrick et al.*, 1993; *Kent et al.*, 1994; *Mutter et al.*, 1995]. Petrologic evidence for fractionation-controlled compositional variations along this part of the EPR also implies the existence of a long-lived AMC [*Sinton et al.*, 1991]. Axial lavas sampled in the study area also show spatial variations in geochemistry corresponding to the structural segmentation of the ridge [*Sinton et al.*, 1991; *Mahoney et al.*, 1994].

Ridge axis morphology appears to be an indicator of magma budget on fast spreading centers [*Macdonald and Fox*, 1988; *Scheirer and Macdonald*, 1993]. The ridge axis depth is shallow (< 2700 m deep) and relatively uniform (~2600-2800 m) from 15˚ to 19˚S, then deepens rapidly approaching the large overlapping spreading center at 20.7˚S [*Scheirer and Macdonald*, 1993]. The cross-sectional area of the axial high increases from a small, triangular high at near 15˚S to a large, domal high with one of the largest cross-sectional areas of any mid-ocean ridge at 17˚-18˚S, suggesting a correspondingly high magma budget, and then decreases to a small, triangular high toward the southern end of the study area [*Scheirer and Macdonald*, 1993]. The off-axis thickness of seismic layer 2A weakly correlates with ridge cross-sectional area at 17°-18°S [*Carbotte et al.*, 1997]. However, this correlation is less certain for the EPR 13°-21°S [*Hooft et al.*, 1997]. The numerous seamount chains in the Rano Rahi Seamount Field, at 16°-19°S, indicate unusually high off-axis magma supply in the study area [*Scheirer et al.*, 1996b].

3. Methods and Definitions

This study catalogues all conical edifices on crust younger than about 1.5-2 Ma on the southern East Pacific Rise from 15.3˚S to 20˚S using the full-coverage multibeam bathymetric data recently obtained in this region [*Scheirer et al.*, 1996a,c] (Figure 2). Using topographic maps derived

from 200 m grids and contoured at 10 m intervals, we picked volcanoes having a minimum of five roughly circular closed contours above the surrounding seafloor (Figure 3). We chose a minimum height of 50 m based on the roughly 10 m vertical resolution of the SeaBeam 2000 multibeam system, the dominant source of bathymetry data in the study area, to mitigate the possibility of picking small multibeam artifacts as volcanoes. Closed-contour artifacts of up to 30 m can appear near the edges of the ~10 km wide swaths [*Kleinrock et al.*, 1992; *Scheirer et al.*, 1996a]. As a result, volcanic edifices under 50 m high are not part of this regional study, although there are some tiny volcanic mounds, less than 20 m high and 100 m in radius, on the axial high [*White et al.*, 1997; R. M. Haymon, unpublished data, Sojourn02 R/V Melville, 1996].

For each volcano, the geographical position of the center of the edifice, the length of base parallel and perpendicular to ridge strike, the length of summit parallel and perpendicular to ridge strike, and the height were measured directly from the maps. The volume of each edifice is calculated by approximating its shape as a truncated right-elliptical cone. Volcanoes are assumed to be nearly circular in plan view, whereas faulted horsts are elongate parallel to the ridge, even where draped by lava flows. Edifices with an aspect ratio >2 elongate with respect to the trend of the ridge axis are likely to be fault blocks rather than volcanoes and were omitted.

From this compilation of all volcanic edifices of 50 m or taller, we define a volcano chain as a group of volcanoes simultaneously satisfying two criteria (Figure 4). First, a volcano chain must consist of three or more edifices with colinear summit areas. Second, the distance between the edge of the base of two adjacent volcanoes in a chain must be less than the basal diameter of the larger volcano of the pair. Classifying a volcano as belonging to a chain implies some connection among the edifices, so this proximity rule was derived empirically to fit the previously identified Rano Rahi volcano chains [*Scheirer et al.*, 1996b] but prevent widely separated but colinear volcanoes from being classified as part of the same volcano chain. The low height cutoff for the volcanoes catalogued in this study introduces a higher spatial density of off-axis volcanoes, compared to previous volcano distribution studies in regions of abundant volcano chains [*Scheirer and Macdonald*, 1995; *Scheirer et al.*, 1996b]. This high spatial density of volcanoes means some volcanoes will be apparently aligned along any random line; so, these criteria are essential to defining which volcanoes comprise chains independent of the size of the volcanoes or the orientation of the chain.

Isolated volcanoes are defined in this study as topographic highs with a minimum height of 50 m, with an aspect ratio ≤ 2, and not identified as a chain-volcano based on the criteria explained above (Figure 3).

Although nearly complete bathymetry is available within the survey area, the abundance and volume of isolated volcanoes were normalized to values per 1000 km^2, excluding the area covered by seamount chains. This minimizes effects of burial of isolated volcanoes by lava flows and mass wasting associated with seamount chains. To determine the age of the crust a volcano resides upon, the magnetic isochron picks in the study area were gridded using a minimum curvature spline [*Smith and Wessel*, 1990] to obtain a grid of the crustal age within the study area incorporating all known magnetic isochrons [*Cormier et al.*, 1996; D. Wilson, personal communication, 1997]. The seafloor age at the location of each volcano was then interpolated from the crustal age grid.

4. General Description of the Volcano Population Near the SEPR

No conical edifices taller than 50 m exist at the summit of the axial high along the entire length of the EPR [*Macdonald et al.*, 1992; *Scheirer and Macdonald*, 1993; *Alexander and Macdonald*, 1996], in striking contrast to the abundant volcanic edifices in the neovolcanic zone of slow or intermediate spreading centers [*Smith and Cann*, 1992; *Kleinrock et al.*, 1994; *Magde and Smith*, 1995; *Smith et al.*, 1995]. Volcanoes 50 m high form immediately off the SEPR axial high, as close as 1 km from the ridge axis, but volcanoes found within 6 km of the axis are mostly adjacent to OSCs. Only 3 of 15 volcanoes found within 6 km of the axis are farther than 15 km from the nearest OSC (Figure 2). Beyond 6 km from the ridge axis, volcanoes are scattered throughout the study area.

This study catalogued 1070 volcanoes (including those in chains) with heights of at least 50 m on ~113,000 km^2 of seafloor. These volcanoes cover 6% of the seafloor in the study area. A total of 680 isolated near-axis volcanoes were identified, and 555 of these volcanoes were less than 100 m high. We found only four isolated near-axis seamounts (volcanoes taller than 1000 m), all located on the Nazca plate from 17˚ to 18˚S beyond 25 km from the axis (Figure 5a). These seamounts contribute a disproportionate amount to the total volume of the isolated near-axis volcanism (Figure 5b). Because the isolated volcanoes have such an uneven size distribution, the median volume represents the typical size of the volcanoes better than the mean. The median volume is used for this reason in all subsequent analyses of isolated volcano size and growth patterns.

In contrast to isolated volcanoes, volcano chains have a much greater proportion of large volcanoes. Over half the 390 chain volcanoes counted in this study are taller than 100 m and 85% of the seamounts (>1000 m high) in the area occur in volcano chains. The seamount chains of the Rano Rahi Seamount Field all have more than one volcanic edifice over 500 m high [*Scheirer et al.*, 1996b]. However, we identified a few new chains on the east flank that are composed entirely of volcanic edifices under 500 m high.

Eruptions from all off-axis volcanoes on crust <2 Ma have increased the volume of the crust by 0.2%, assuming a uniform 6 km thick crust. This estimate of off-axis volcanic contribution to the crust is a lower limit because lava flows that do not create a volcanic edifice at least 50 m high are not included in these values. Many of the larger volcanoes, especially the volcano chains, are built upon platforms, up to a few tens of meters high, presumably made up of basaltic flows related to the edifices that sit atop them (Figures 3 and 4). These platforms were not included in the our volume or area estimates because they failed to meet the closed-contour or aspect-ratio criteria for volcanoes. However, a conservative estimate of their areal extent would double the amount of seafloor covered by flows from the isolated volcanoes, and significantly increase our estimate of the contribution from near-axis volcanoes to the volume of the crust.

Of the 555 volcanoes 50-100 m in height, 9 have craters large enough to show up on 200 m gridded bathymetry maps, 85 are irregular or "hat-shaped" [*Smith et al.*, 1995; *Head et al.*, 1996], and the remaining are dome shaped (Figure 3b). Assuming these small off-axis volcanoes form entirely by the eruption of basalt with pillow morphology (rather than by mixed intrusive/extrusive activity), we can estimate a minimum time of formation of 2-10 days of continuous eruption given a typical lava flux of 10-100 m^3/s for pillows to form [*Gregg and Fink*, 1995]. The largest isolated volcanoes with volumes exceeding 30 km^3 would take at least 10 years of continuous eruption to form at a lava flow rate of 100 m^3/s. At least some of these volcanoes probably form in a series of eruptions punctuated by pauses or intrusive activity [*Lonsdale*, 1983]. While submarine eruptions have never been observed, subaerial cinder cones, spatter cones, littoral cones, and vent craters have been observed to form in a matter of hours to days [e.g., *Thorarinsson*, 1969; *Holcomb*, 1987; *Lockwood et al.*, 1987]. Formation of similar-sized submarine volcanoes may occur on a generally similar timescale, making a period of 2-10 days a reasonable order-of-magnitude estimate.

5. Distribution of Isolated Volcanoes Across and Along the Axis

Owing to asymmetric spreading in the study area, seafloor crustal age does not correspond directly to the distance off-axis in the study area (Figure 2). Therefore we binned the population of isolated near-axis volcanoes in 0.1 Myr crustal age intervals, overlapping by 0.05 Myr, running the length of the study area, incorporating the local spreading asymmetries [*Cormier et al.*, 1996]. When plotted in 0.1 Myr bins as a function of crustal age, the numbers of isolated volcanoes reach their long-term averages by 0.2 Myr (Figure 6a). Also, the overall abundance of isolated near-axis volcanoes is symmetric about the ridge, in contrast to the extremely asymmetric distribution of the volcano chains (Figure 2). Although the data are noisy, a steady median volume is reached in the first bin from the ridge axis (Figure 6b). The observation that the median volume of isolated near-axis volcanoes remains constant with distance from the axis indicates that typical isolated volcanoes erupt most of their volume within the time span of one age bin, less than 0.1 Myr (Figure 6b). That the timespan of the edifice building stage is not resolvable with 0.1 Myr bins is not surprising based on our inference of a time span of days to weeks for the main eruptive activity of typical isolated volcanoes.

Several complications can obscure the distribution of isolated volcanoes with respect to crustal age. Seamount chains and their debris aprons may overprint the isolated volcanoes [*Scheirer et al.*, 1996b], as dealt with previously. Also, largely uninvestigated basaltic sheet flows and normal faulting may contribute to an apparent decrease in abundance of volcanoes beyond their initial zone of formation by mass wasting and burial. Finally, sediment accumulation could bury volcanic edifices, but this is not a significant factor in our study area. Sedimentation rates of 3-6 m/Myr are typical of recent estimates for this area [*Marchig et al.*, 1986; *Lyle et al.*, 1987; *Dekov and Kuptsov*, 1992]. This could lead to undersampling of smaller edifices at the outer edge of the study area, where 10 m of sediments could be deposited. For crust younger than 1 Ma, the deposition of less than 6 m of sediment is not likely to change the overall distribution of ≥50 m high edifices. No systematic correction to the across-axis distribution data was made for increasing sediment thickness because the < 5 m uncertainty is beyond the resolution of the multibeam bathymetry data.

Along the axis, there is a transition at 19˚S from abundant seamount chains to the north to an area without any volcano chains to the south where only small isolated volcanoes are found (Figure 2). The ridge axis depth increases, and the cross-sectional area, a proxy for axial magma budget, decreases significantly near this transition [*Scheirer and Macdonald*, 1993](Figure 7). A similar correlation

between greater seamount volcanism and larger cross-sectional area of the axial high was also found for the EPR 8°-18°N [*Scheirer and Macdonald*, 1995] and for the EPR near the Wilkes Fracture Zone [*Keeley et al.*, 1995]. Isolated near-axis volcanoes occur everywhere along the axis on both sides of the ridge, 15˚-20˚S, and the magma supply to both the ridge axis and the isolated near-axis volcanoes may be related.

To investigate along-axis correlations between the isolated volcanoes and ridge-axis morphology, we used quarter-degree latitude bins (28 km) extending 20 km to both sides of the axis (crust <0.25 Ma). These bins sample enough volcanoes per bin (>5) to be statistically meaningful but encompass a short period of time so that we may assume the cross-sectional area of the ridge has not changed significantly [*Scheirer and Macdonald*, 1993]. The total volume of isolated volcanoes correlates well with the average axial cross-sectional area (Figure 8a). However, fewer isolated volcanoes per unit area are found where the axial cross-sectional area is highest (Figure 8b). Thus a relatively narrow ridge is associated with many small isolated volcanoes, while fatter ridge segments have a smaller number of larger volcanoes with a greater total volume contribution. In the areas with a low volume of isolated near-axis volcanoes but a large axial cross-section (Figure 8a), volcano chains are the dominant expression of off-axis volcanism.

In agreement with these correlations, volcanoes from 19˚ to 20˚S are more abundant (10 compared to 7 per 1000 km^2) and generally smaller (median volume of 0.015 km^3 compared to 0.026 km^3) than for the study area as a whole. However, the width of the isolated volcano formation zone from 19˚ to 20˚S remains the same as for the entire area (Figures 9a and 9b).

In contrast to the observed correlation between axial cross-sectional area and volcano volume, ridge depth and volcano volume show a weaker correlation. This may result from the small variation in axial depth along most of the study area [*Scheirer and Macdonald*, 1993]. The depth of the AMC reflector below the axis [*Detrick et al.*, 1993] is not related to the total volume of nearby isolated volcanoes. Cross-sectional area of the ridge axis probably averages the magma budget over >0.1 Myr, whereas the depth to the AMC reflector may vary over a shorter time [*Scheirer and Macdonald*, 1993; *Carbotte et al.*, 1997; *Hooft et al.*, 1997]. Using a 40 km wide corridor centered on the ridge axis averages the off-axis volcanism over 0.25 Myr. It would be interesting to see if there is a correlation between areas of enhanced off-axis volcanism and areas along the axis that are underlain by axial magma chambers with a high percentage of melt. No correlation is evident based on the small

area studied near 14°S [*Singh et al.*, 1997]. We suspect that the timescale of change for the axial magma lens is short compared to the ~0.2 Myr time interval for the eruption of near-axis volcanoes but await further seismic analysis.

6. Height Distribution of Near-Axis Volcanoes

To compare the distribution of volcanoes in this study with the characteristic seamount heights and areal densities of other studies, volcano height distribution parameters are calculated using maximum likelihood regression [*Smith and Jordan*, 1988]. An exponential distribution is fit to the isolated volcano height distribution, binned in 10 m height intervals from 50 to 350 m with at least five volcanoes per bin. This study predicts a characteristic height of 28 m with an areal density of 31 edifices per 1000 km^2 for the population of small isolated volcanoes and a characteristic height of 106 m with an areal density of 6 edifices per 1000 km^2 for volcano chains, including the smaller volcano chains. For seamounts >200 m high in the Rano Rahi Seamount Field, the maximum likelihood regression predicts a characteristic height of 295 m and areal distribution of 9.5 edifices per 1000 km^2 [*Scheirer et al.*, 1996b]. The distinct distributions suggest that isolated volcanoes and volcano chains comprise two separate populations (Figure 10 and Table 1). Comparing their height distribution parameters, isolated volcanoes erupting off-axis on fast spreading ridges and the axial volcanic cones at slow spreading ridges also form two distinct populations (Table 1).

7. Isolated Volcano Formation and Lithospheric Thickness

One of the controversies regarding submarine volcano formation is whether melt supply or lithospheric penetrability controls off-axis volcanism [e.g., *Vogt*, 1974; *Batiza*, 1981, 1982; *Fornari and Luckman*, 1987]. The width of the zone of isolated volcano formation may be relevant to this problem. We found that the zone of initial formation of isolated volcanoes on the southern EPR extends out to 0.2 Ma crust on either flank (Figure 6a). Along a segment of the northern EPR, *Alexander and Macdonald* [1996] concluded the zone of formation for small off-axis volcanoes is 10-20 km wide, also corresponding to a crustal age of 0.1-0.2 Ma. On the Mid-Atlantic Ridge (MAR), most axial volcanoes occur in a zone with a total width of about 4 km, again corresponding to a crustal age of roughly 0.2 Ma [*Smith and Cann*, 1992]. The common 0.2 Ma limit on the width of isolated volcano formation suggests lithospheric penetrability controls where new isolated volcanoes form.

Neither within our study area nor on the northern EPR [*Alexander and Macdonald*, 1996] was there any demonstrable association between the abyssal hill normal faults and off-axis volcanism. The only obvious linear alignment of volcanoes was found perpendicular to the trend of the seafloor fault fabric (Figure 2), suggesting that preexisting lines of weakness along faults play a secondary role in determining the near-axis volcano distribution. Stresses generated by the magma source are the most probable primary control on the distribution of isolated near-axis volcanoes.

Perhaps the depth to the brittle-ductile transition in oceanic lithosphere controls the width of the zone of initiation of isolated volcanoes. Once the brittle lid reaches a sufficient thickness to prevent dikes from either initiating or erupting, new volcanoes stop forming. The ambient stresses at the dike tip and thermal diffusivity at the dike walls principally limit the ability of magma to propagate upward through the brittle lid and erupt [*Rubin*, 1995]. In simple terms, the magma pressure must overcome the elastic stiffness of the overlying rock and the local compressive stress perpendicular to the fracture plane to initiate a fracture for propagation of a dike [*Secor and Pollard*, 1975]. Presumably, a magma body of constant size will have greater difficulty initiating a crack at the base of thicker brittle lithosphere because the mean normal stress across dike-induced cracks increases with depth. On the basis of the small size of most isolated volcanoes, we speculate that they originate from rather small magma bodies incapable of penetrating a thick brittle lid.

Even when one of these small magma lenses produces a dike, thermal stresses generated by underplating new, hot material to the base of cooler lithosphere would cause relative compression at the top of the plate, as the base of the plate cools and contracts faster than the older lithosphere above it [*Bratt et al.*, 1985; *Wessel*, 1992]. This relative compressional stress at the top of the plate may increase in magnitude with lithospheric age for rapidly thickening lithosphere (< 100 Ma) and impede the ascent of dikes through older lithosphere. It is worth noting that many volcano chains on the EPR also appear to initiate within 0.2 Myr of the ridge axis, although they experience most of their volume increase farther off-axis [*Scheirer and Macdonald*, 1995; *Scheirer et al.*, 1996b]. Local heating of the lithosphere associated with seamount chains may decrease the usual rate of lithospheric thickening, producing a melt channel effect that may allow continued volcanic activity farther off-axis near previously active eruptive centers.

To estimate the depth to the brittle-ductile transition at different spreading rates, we use a simple one-dimensional thermal model of lithospheric cooling that increases the depth of the isotherm with square root of crustal age from the axis [*Turcotte and Schubert*, 1982]. The simple model was modified to include information about the axial thermal structure by adding the depth to the low-velocity zone calculated by *Purdy et al.* [1992], which displaces the isotherms downward. Although we acknowledge this model is simplistic, it gives a straightforward approximation of the thickness of the brittle lithosphere. The model suggests that a brittle lid thickness of ~4-6 km (or the mean normal stresses across potential cracks at the base of lithosphere of this thickness) is sufficient to block the formation of new isolated volcanoes at all three spreading rates (Figure 11). In comparison, the thermal model of *Wilson et al*. [1988] that includes cooling at the base and the top of a convecting magma chamber for the fast spreading EPR places the brittle-ductile transition at a depth of roughly 3 km below the surface of 0.2 Ma lithosphere. If the thermal model of *Phipps Morgan and Chen* [1993] is used at these three spreading rates, the thickness of brittle lithosphere becomes roughly 8 km in the zone of isolated volcanoes formation. So, while the exact thickness is model-specific, the influence of lithospheric thickness on dike-induced cracking of the brittle lid may limit how far off axis isolated volcanoes form at all spreading rates.

8. Hypotheses for the Origin of Isolated Near-Axis Volcanoes (and Suggestions for Future Work)

On the basis of the spatial distribution of volcanoes, formation of isolated volcanoes appears to be a steady state process related to axial magmatic upwelling, whereas volcano chains seem more consistent with formation by sporadic eruption of lavas derived from mantle heterogeneities as envisioned by *Wilson* [1992] and *Davis and Karsten* [1986]. To explain the distribution of isolated near-axis volcanoes, low volume eruptions must occur on an almost steady state basis in the near-axis region. We speculate that a possible record of the magmatic processes creating isolated near-axis volcanoes may be preserved as late stage wehrlitic intrusions and uppermost ankaramitic lavas in ophiolites [*Juteau et al.*, 1988; C. A. Hopson and J. Mattinson, Wehrlitic magma series and ultramafic transition zone, Point Sal remnant of the Coast Range ophiolite: Implications for ocean ridge off-axis volcanism, manuscript in preparation, 1998]. If the isolated near-axis volcanoes tap such a source as their magma supply, they should be generally more primitive and depleted than tholeiitic lavas on the adjacent ridge segment, a prediction testable by collecting rock samples from the smaller near-axis volcanoes.

The first appearance of off-axis volcanoes along the EPR from 9˚10'-9˚50'N is just beyond 5 km from the axis; however, that study excluded seafloor near OSCs [*Alexander and Macdonald*, 1996]. Along the EPR from 15.3˚ to 20˚S, the few volcanoes within 6 km of the ridge are near OSCs (Figure 2). Formation of isolated near-axis volcanoes seems to be common within the discordant zones created by OSCs all along the EPR. For example, ridge 4 on the 20˚40'S OSC is a prominent volcanic feature [*Macdonald et al.*, 1988], and volcanic edifices occur on abandoned ridge tips near 20˚S, 114˚30'W [*Macdonald et al.*, 1988]; 17˚05'S, 112˚20'W [*Scheirer et al.*, 1996]; 9˚N [*Macdonald et al.*, 1992]; 11˚45'N [*Perram and Macdonald*, 1990]; and 12˚54'N [*Antrim et al.*, 1988]. Constructional volcanoes may form at abandoned ridge tips as melt pockets become isolated by the "self-decapitation" of the propagating ridge as spreading stops on the abandoned segment [*Macdonald et al.*, 1987]. Geochemistry of basalt samples from OSCs along the southern EPR shows that ridge offsets tend to erupt more fractionated magma [*Sinton et al.*, 1991]. Sampling of the small volcanic cones near OSCs would be the best way to confirm their origin, leading to better understanding of the subcrustal processes at ridge discontinuities. At present, such sampling has not been done at the resolution necessary to address these questions.

9. Conclusions

The distribution of isolated off-axis volcanoes on the ultrafast spreading EPR, 15.3˚-20˚S, suggests that ridge volcanism at fast spreading rates is not confined to the axis. While the abundant volcano chains west of the axis imply that an asymmetric off-axis magma supply creates most seamounts and large volcanoes, near-axis isolated volcanoes are equally abundant on both sides of the ridge. The median volume of isolated volcanoes remains nearly constant as a function of distance from the ridge, indicating the majority of isolated volcanoes do not grow significantly beyond 0.2 Ma crustal age. The total volume of isolated volcanoes appears to increase where the ridge has a larger cross-sectional area and hence higher magma supply. The inferred width of the zone of volcano formation increases with spreading rate for near-axis volcanism on the MAR, northern EPR, and southern EPR, such that isolated volcanoes form only on lithosphere less than 0.2 Myr old in all cases, suggesting a lithospheric control on production of isolated volcanoes near ridges.

References

Alexander, R. T., and K. C. Macdonald, Small off-axis volcanoes on the East Pacific Rise, Earth Planet. Sci. Lett., 139, 387-394, 1996.

Antrim, L., J.-C. Sempere, K. C. Macdonald, and F. N. Spiess, Fine scale study of a small overlapping spreading center system at 12°54'N on the East Pacific Rise, *Mar. Geophys. Res., 9,* 115-130, 1988.

Batiza, R., Lithospheric age dependence on the rate of off-ridge volcano production in the North Pacific, *Geophys. Res. Lett., 8,* 853-856, 1981.

Batiza, R., Abundance, distribution and sizes of volcanoes in the Pacific Ocean and implications for the origin of non-hotspot volcanoes, *Earth Planet. Sci. Lett., 60,* 196-206, 1982.

Bemis, K. G., and D. K. Smith, Production of small volcanoes in the Superswell region of the South Pacific, *Earth Planet. Sci. Lett., 118,* 251-263, 1993.

Bratt, S. R., E. A. Bergman, and S. C. Solomon, Thermoelastic stress: How important as a cause of earthquakes in young oceanic lithosphere?, *J. Geophys. Res, 90,* 10249-10260, 1985.

Carbotte, S., J. C. Mutter, and L. Xu, Contribution of tectonism and volcanism to axial and flank morphology of the southern East Pacific Rise from a study of layer 2A geometry, *J. Geophys. Res., 102,* 10165-10185, 1997.

Cochran, J. R., Variations in subsidence rates along intermediate and fast spreading mid-ocean ridges, *Geophys. J. R. Astron. Soc., 87,* 421-454, 1986.

Cormier, M.-H., and K. C. Macdonald, East Pacific Rise 18°S-19°S: Asymmetric spreading and ridge reorientation by ultrafast migration of ridge axis discontinuities, *J. Geophys. Res., 99,* 543-564, 1994.

Cormier, M.-H., D. S. Scheirer, and K. C. Macdonald, Evolution of the East Pacific Rise at 16°-19°S since 5 Ma: Bisection of OSC's by new rapidly propagating ridge segments, *Mar. Geophys. Res., 18,* 52-84, 1996.

Davis, E. E., and J. L. Karsten, On the cause of the asymmetric distribution of seamounts about the Juan de Fuca Ridge: Ridge crest migration over a heterogenous asthenosphere, *Earth Planet. Sci. Lett., 79,* 385-396, 1986.

Dekov, V. M., and V. M. Kuptsov, Late quarternary rates of accumulation of metal-bearing sediments on the East Pacific Rise, *Oceanology, 32,* 94-101, 1992.

Detrick, R. S., A. J. Harding, G. M. Kent, J. A. Orcutt, J. C. Mutter, and P. Buhl, Seismic structure of the southern East Pacific Rise, *Science, 259,* 499-503, 1993.

Fornari, D., and M. A. Luckman, Seamount abundances and distribution near the East Pacific Rise 0-24°N based on Seabeam data, in *Seamounts, Islands and Atolls, Geophys. Monogr. Ser., vol.* 43, edited by B. Kaeting, P. Fryer, R. Batiza and T. J. Boehler, pp. 13-21, Washington, D.C., 1987.

Forsyth, D. W., S. C. Webb, L. M. Dorman, and Y. Shen, Phase volocities of Rayleigh waves in the MELT experiment on the East Pacific Rise, *Science, 280,* 1235-1238, 1998.

Gregg, T. K. P., and J. H. Fink, Quantification of submarine lava-flow morphology through analog experiments, *Geology, 23,* 73-76, 1995.

Head, J. W., L. Wilson, and D. K. Smith, Mid-ocean ridge eruptive vent morphology and structure: Evidence for dike widths, eruption rates, and evolution of eruptions and axial volcanic ridges, *J. Geophys. Res., 101,* 28265-28280, 1996.

Holcomb, R. T., Eruptive history and long-term behavior of Kilauea Volcano, in *Volcanism in Hawaii,* edited by R. W. Decker, T. L. Wright, and P. H. Stauffer, *U.S. Geol. Surv. Prof. Pap., 1350,* 261-350, 1987.

Hooft, E. E., R. S. Detrick, and G. M. Kent, Seismic structure and indicators of magma budget along the Southern East Pacific Rise, *J. Geophys. Res., 102,* 27319-27340, 1997.

Juteau, T., M. Ernewein, I. Rueber, H. Whitechurch, and R. Dahl, Duality of magmatism in the plutonic sequence of the Sumail nappe, Oman, *Tectonophysics, 151,* 107-135, 1988.

Keeley, C. D., A. Marcario, W. F. B. Ryan, and W. F. Haxby, Simulating seamount populations for the sourthern East Pacific Rise and the Pacific/Antarctic Ridge, *Eos Trans. AGU 76* (16), Spring Meet. Suppl., 273, 1995.

Kent, G. M., A. J. Harding, J. A. Orcutt, R. S. Detrick, J. C. Mutter, and P. Buhl, The uniform accretion of oceanic crust south of the Garrett Transform at 14°15'S on the East Paicific Rise, *J. Geophys. Res., 99,* 9097-9116, 1994.

Kleinrock, M. C., R. N. Hey, and A. E. Theberge, Practical geological comparison of some seafloor survey instruments, *Geophys. Res. Lett., 19,* 1407-1410, 1992.

Kleinrock, M. C., B. A. Brooks, and D. K. Smith, Construction and destruction of volcanic knobs at the Cocos-Nazca spreading system near 95°W, *Geophys. Res. Lett., 21,* 2307-2310, 1994.

Lockwood, J. P., J. J. Dvorak, T. T. English, R. Y. Koyanagi, A. T. Okamura, M. L. Summers, and W. R. Tanigawa, Mauna Loa 1974-1984; A decade of intrusive and extrusive activity, in *Volcanism in Hawaii,* edited by R. W. Decker, T. L. Wright, and P. H. Stauffer, *U.S. Geol. Surv. Prof. Pap., 1350,* 537-570, 1987.

Lonsdale, P., Laccoliths(?) and small volcanoes on the flank of the East Pacific Rise, *Geology, 11,* 706-709, 1983.

Lonsdale, P., Segmentation of the Pacific-Nazca spreading center, 1°N-20°S, *J. Geophys. Res., 94*, 12197-12226, 1989.

Lyle, M., M. Leinen, R. M. Owen, and D. K. Rea, Late Tertiary history of hydrothermal deposition at the East Pacific Rise, 19°S: Correlation to volcano-tectonic events, *Geophys. Res. Lett., 14*, 595-598, 1987.

Macdonald, K. C., J.-C. Sempere, P. J. Fox, and R. Tyce, Tectonic evolution of ridge axis discontinuities by the meeting, linking, or self-decapitation of neighboring ridge segments, *Geology, 15*, 993-997, 1987.

Macdonald, K. C., and P. J. Fox, The axial summit graben and cross-sectional shape of the East Pacific Rise as indicators of axial magma chambers and recent volcanic eruptions, *Earth Planet. Sci. Lett., 88*, 119-131, 1988.

Macdonald, K. C., R. M. Haymon, S. P. Miller, J.-C. Sempere, and P. J. Fox, Deep-Tow and Sea Beam studies of dueling propagating ridges on the East Pacific Rise near 20˚40'S, *J. Geophys. Res., 93*, 2875-2898, 1988.

Macdonald, K. C., P. J. Fox, S. Carbotte, M. Eisen, S. Miller, L. Perram, D. Scheirer, S. Tighe, and C. Weiland, The East Pacific Rise and its flanks, 8°-18°N: History of segmentation, propagation and spreading direction based on SeaMARC II and Sea Beam studies, *Mar. Geophys. Res., 14*, 299-344, 1992.

Macdonald, K. C., P. J. Fox, R. T. Alexander, R. Pockalny, and P. Gente, Volcanic growth faults and the origin of Pacific abyssal hills, *Nature, 380*, 125-129, 1996.

Magde, L. S., and D. K. Smith, Seamount volcanism at the Reykjanes Ridge: Relationship to the Iceland hot spot, *J. Geophys. Res., 100*, 8449-8468, 1995.

Mahoney, J. J., J. M. Sinton, M. D. Kurz, J. D. Macdougall, K. J. Spencer, and G. W. Lugmair, Isotope and trace element characteristics of a super-fast spreading ridge: East Pacific Rise, 13°-23°S, *Earth Planet. Sci. Lett., 121*, 173-193, 1994.

Marchig, V., J. Erzinger, and P. M. Heinze, Sediment in the black smoker area of the East Pacific Rise, *Earth Planet. Sci. Lett., 79*, 93-106, 1986.

MELT Seismic Team, Imaging the deep seismic structure beneath a mid-ocean ridge: The MELT Experiment, *Science, 280*, 1215-1218, 1998.

Mutter, J. C., S. M. Carbotte, W. Su, L. Xu, P. Buhl, R. S. Detrick, G. Kent, J. Orcutt, and A. Harding, Seismic images of active magma systems beneath the East Pacific Rise 17° to 17°35'S, *Science, 268,* 391-395, 1995.

Perram, L. J., and K. C. Macdonald, A one-million-year history of the 11°45'N East Pacific Rise discontinuity, *J. Geophys. Res., 95,* 21,363-21,381, 1990.

Phipps Morgan, J., and Y. J. Chen, The genesis of oceanic crust: Magma injection, hydrothermal circulation and crustal flow, *J. Geophys. Res., 98,* 6283-6297, 1993.

Purdy, G. M., L. S. L. Kong, G. L. Christeson, and S. C. Solomon, Relationship between spreading rate and the seismic structure of mid-ocean ridges, *Nature, 355,* 815-817, 1992.

Rappaport, Y., D. F. Naar, C. C. Barton, Z. J. Liu, and R. N. Hey, Morphology and distribution of seamounts surrounding Easter Island, *J. Geophys. Res., 102,* 24713-24728, 1997.

Rubin, A. M., Propagation of magma-filled cracks, *Annu. Rev. Earth Planet. Sci., 23,* 287-336, 1995.

Scheirer, D. S., and K. C. Macdonald, Variation in cross-sectional area of the axial ridge along the East Pacific Rise: Evidence for the magamatic budget of a fast-spreading center, *J. Geophys. Res., 98,* 7871-7885, 1993.

Scheirer, D. S., and K. C. Macdonald, Near-axis seamounts on the flanks of the East Pacific Rise, 8°N to 17°N, *J. Geophys. Res., 100,* 2239-2259, 1995.

Scheirer, D. S., K. C. Macdonald, D. W. Forsyth, S. P. Miller, D. W. Wright, and M.-H. Cormier, A map series of the southern East Pacific Rise and it's flanks, 15°S to 19°S, *Mar. Geophys. Res., 18,* 1-12, 1996a.

Scheirer, D. S., K. C. Macdonald, D. W. Forsyth, and Y. Shen, Abundant seamounts of the Rano Rahi seamount field near the southern East Pacific Rise, 15º to 19ºS, *Mar.Geophys.Res., 18,* 13-52, 1996b.

Scheirer, D. S., M. H. Cormier, K. C. Macdonald, R. M. Haymon, S. M. White, and Sojn01 Sci. Party, Completing the picture of the East Pacific Rise and its flanks in the MELT area, *Eos Trans. AGU, 77*(44), Fall Meet. Suppl., 663, 1996c.

Scheirer, D. S., D. W. Forsyth, M.-H. Cormier, and K. C. Macdonald, Shipboard geophysical indications of asymmetry and melt production beneath the East Pacific Rise near the MELT Experiment, *Science, 280,* 1221-1224, 1998.

Secor, D. T., and D. D. Pollard, On the stability of open hydraulic fractures in the Earth's crust, *Geophys. Res. Lett., 2,* 510-513, 1975.

Shen, Y., D. S. Scheirer, D. W. Forsyth, and K. C. Macdonald, Trade-off in production between adjacent seamount chains near the East Pacific Rise, *Nature, 373,* 140-143, 1995.

Singh, S. C., J. Collier, G. Kent, and A. Harding, Along-axis variations in crustal magma properties at the southern East Pacific Rise: Melt to mush, *Eos Trans. AGU, 78*(46), Fall Meeting. Suppl., 670, 1997.

Sinton, J. M., S. M. Smaglik, J. J. Mahoney, and K. C. Macdonald, Magmatic processes at superfast spreading mid-ocean ridges: Glass compositional variations along the East Pacific Rise 13°-23°S, *J. Geophys. Res., 96,* 6133-6155, 1991.

Smith, D. K., J. R. Cann, M. E. Dougherty, J. Lin, S. Spencer, C. MacLeod, J. Keeton, E. McAllister, B. Brooks, R. Pascoe, and W. Robertson, Mid-Atlantic Ridge volcanism from deep-towed side-scan sonar images, 25-29N, *J. Volc. Geotherm. Res., 67,* 233-262, 1995.

Smith, D. K., and J. R. Cann, The role of seamount volcanism in crustal construction at the Mid-Atlantic Ridge (24°30'N), *J. Geophys. Res., 97,* 1645-1658, 1992.

Smith, D. K., and T. H. Jordan, Seamount statistics in the Pacific Ocean, *J. Geophys. Res., 93,* 2899-2918, 1988.

Smith, W. H. F., and P. Wessel, Gridding with continuous curvature splines in tension, *Geophysics, 55,* 293-205, 1990.

Thorarinsson, S., The Lakagigar eruption of 1783, *Bull. Volcanol., 33,* 910-927, 1969.

Turcotte, D. L., and G. Schubert, *Geodynamics Applications of Continuum Physics to Geological Problems,* 450 pp., John Wiley, New York, 1982.

Vogt, P. R., Volcano spacing, fractures, and thickness of the lithosphere, *Earth Planet. Sci. Lett., 21,* 235-252, 1974.

Wessel, P., Thermal stresses and the bimodal distribution of elastic thickness estimates of oceanic lithosphere, *J. Geophys. Res., 97,* 14177-14193, 1992.

White, S. M., K. C. Macdonald, D. S. Scheirer, M.-H. Cormier, and R. M. Haymon, Isolated Near-Axis Volcanoes on the SEPR: Is the neovolcanic zone 28km wide?, *Eos Trans. AGU, 78*(46), Fall Meet. Suppl., 689, 1997.

Wilson, D. S., Focused mantle upwelling beneath mid-ocean ridges: Evidence from seamount formation and isostatic compensation of topography, *Earth Planet. Sci. Lett., 113,* 41-55, 1992.

Wilson, D. S., D. A. Clague, N. H. Sleep, and J. L. Morton, Implications of magma convection for the size and temperature of magma chambers at fast spreading ridges, *J. Geophys. Res., 93,* 11974-11984, 1988.

Figure Captions

Figure 1. Shaded relief map, from a 1 km grid illuminated from northwest, of the bathymetric coverage for the flanks of the southern East Pacific Rise. The study area is outlined, and the general location of Rano Rahi Seamount Field is labeled. Inset shows the oceanic plates of the eastern Pacific with the study area shaded.

Figure 2. Shaded-relief map of 1 km grid of bathymetry of the study area (illuminated from NW) with the ridge axis, 0.2 Ma, and 1.0 Ma isochrons drawn as solid lines. Circles show isolated near-axis volcanoes with stars over volcanoes within 6 km of the ridge axis. Symbols are scaled according to the approximate basal diameter of the edifice, but smaller edifices are shown with symbol size larger than their actual diameter at this map scale. Straight lines are drawn over volcano chains.

Figure 3a. Map of ~410 km^2 on ~1.5 Ma Nazca crust. Typical isolated near-axis volcanoes, at least 50 m in height and roughly circular in plan view, are outlined in bold. Contour interval is 10 m on a 200 m grid. Some of these small volcanoes appear to be aligned along the abyssal hills, although they do not form a volcano chain as defined in the text. Several of these volcanoes are built upon platforms, presumably produced by off-axis eruptions.

Figure 3b. Same as Figure 3a, except for ~320 km^2 of ~0.2 Ma Pacific crust.

Figure 4. A typical east flank volcano chain in 3-D persepective, vertical exaggeration of 5X, 100 m contours. Volcano chains consist of several colinear edifices, typically sitting atop a plateau-like base. The largest volcano is 1400 m high with a ~15 km^2 base.

Figure 5. Scattergraphs of (a) height of individual edifices versus distance from the axis and (b) semilog volumes of each edifice versus distance from the axis. Negative distance from the ridge corresponds to west (Pacific) flank. Most of the isolated near-axis volcanoes are small edifices, only a few of which have been catalogued in previous studies.

Figure 6. (a) Number of volcanic edifices found on 1000 km^2 of seafloor not covered by volcano chains. Histogram bins are 0.1 Myr wide and overlap by 0.05 Myr. (b) The median volume of volcanic edifices in the same bins used previously for volcano abundance. Vertical bars show the range from the 25th to 75th percentiles of edifice volumes, illustrating both the wide scatter and the skewness in the volume distribution of isolated volcanoes. The median volume shows no significant changes, suggesting isolated volcanoes typically form in <0.1 Myr, then do not continue to grow.

Figure 7. (top) Total number of volcanoes in quarter-degree latitude bins, 40 km wide, and centered

on the axis. Isolated volcano abundances are normalized for the area covered by seamount chains in each bin. (middle) Cross-sectional area of the ridge axis from *Scheirer and Macdonald*(1993). (bottom) Map view of the axis showing the corridor used to correlate to the axis. Volcano chains are found only where the cross-sectional area ≥4 km^2, but isolated volcanoes are found along the entire ridge and increase in number from 19˚ to 20˚S, where seamount chains are absent.

Figure 8. Correlation of isolated near-axis volcanoes to axial morphology in 15' along-axis by 40 km wide axis-centered bins. (a) Cumulative edifice volume and (b) abundance of volcanoes with respect to the average axial cross-sectional area with 2-sigma error bars about the mean area. Increasing volume of near-axis volcanism seems to correlate with increasing axial cross-sectional area, and increasing numbers of near-axis volcanoes seem to correlate with decreasing axial area.

Figure 9. (a) Abundance and (b) median volume of isolated volcanoes from 19˚S to 20˚S (binned and normalized as in Figure 6), a region of full bathymetric coverage and no volcano chains or large volcanic edifices. This smaller region shows the same general trends as the whole study area but has more volcanic edifices and a smaller median edifice volume.

Figure 10. Maximum likelihood regression predictions of numbers of volcanoes per 1000 km^2 based on cumulative volcano height distribution. Triangles show isolated volcanoes with solid line fit to data in height range of 50-350 m. Circles are volcano chains catalogued in this study with dashed line fit to data in 50-600 m height range. The distribution for the Rano Rahi Seamount Field contains a higher concentration of large volcanoes but uses a height range of 200-1200 m and primarily west flank coverage.

Figure 11. Comparison of calculated depth to the 600˚C isotherm to off-axis distance for the maximum half-width of the zone of volcano formation for the isolated near-axis volcanoes on the southern East Pacific Rise (SEPR) (this study), the northern East Pacific Rise (NEPR) [*Alexander and Macdonald*, 1996] and the Mid-Atlantic Ridge (MAR) [*Smith and Cann*, 1992]. Assuming the brittle-ductile transition occurs at the 600˚C isotherm, new isolated volcanoes appear to form when the brittle lid is less than 4-6 km thick (shaded region). The mean normal stress across any cracks at a depth of 4-6 km at the base of the lithosphere would be ~0.12-0.18 MPa.

Table 1. Seafloor Volcano Height Distribution

Study Area	Height Range, m	β, km^{-1}	Characteristic Height, m	ν $(1000\ km^2)^{-1}$	Source
		Isolated Volcano Areas			
15.3˚-20˚S EPR	50-350	35.9±0.2	30	31.1±.1	This study
S. Pacific "superswell"	50-210	15.9±0.6	62	33±2	*Bemis and Smith* [1993]
95˚W Galapagos	50-315	34.5±2.5	30	370±30	*Kleinrock et al.* [1994]
24˚-30˚N MAR	50-650	17.2±0.5	60	195±9	*Smith and Cann* [1992]
57˚-62˚N Reykjanes	50-300	14.3±0.5	70	310±20	*Magde and Smith* [1995]
		Seamount Chain Areas			
15.3˚-20˚S EPR	50-600	9.4±0.4	110	6.0±0.1	This study
15˚-19˚S EPR	300-1200	3.4±0.1	290	9.5±0.4	*Scheirer et al.* [1996]
8˚-17˚N EPR	200-800	4.3±0.2	230	1.9±0.2	*Scheirer and Macdonald* [1995]
27˚-29˚S EPR	200-1000		308	2.7±0.15	*Rappaport et al.* [1997]

Fitting $\nu = \nu_0 \exp(-\beta H)$.

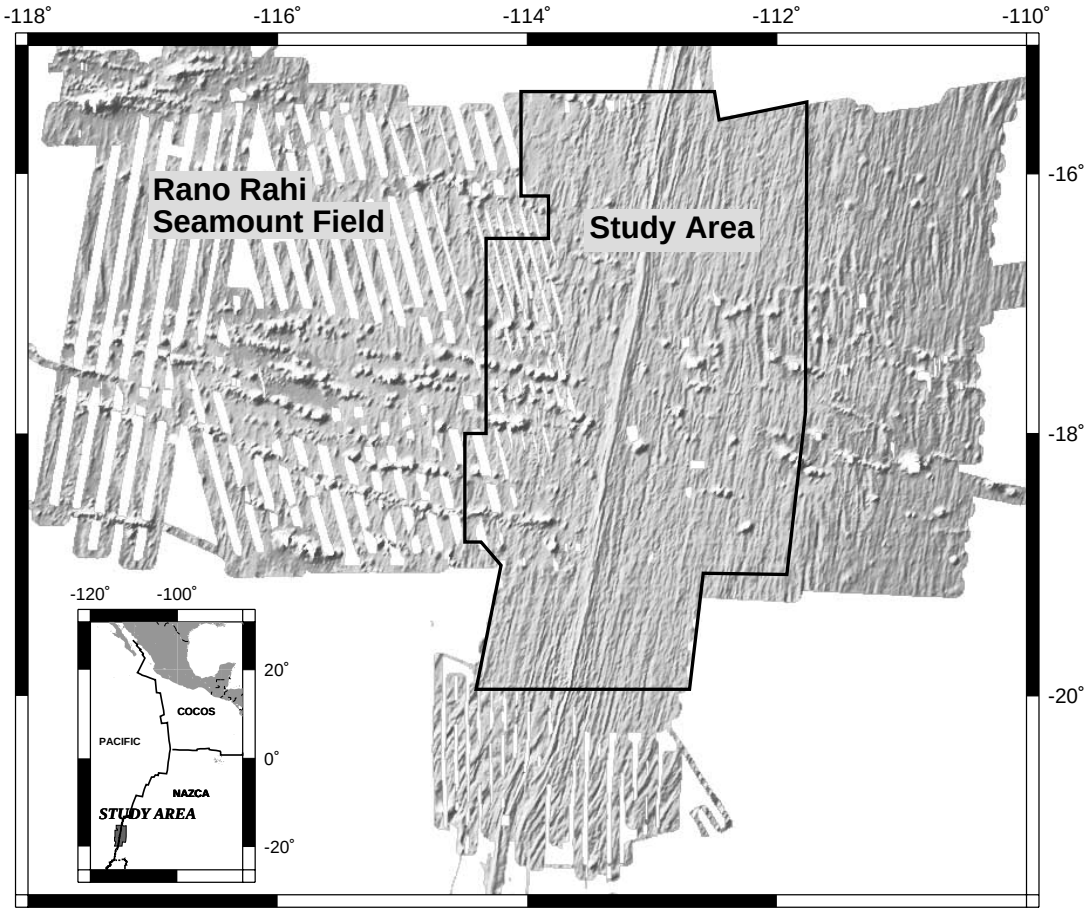
-118˚
-116˚
-114˚
-112˚
-110˚
-16˚
-18˚
-20˚
Rano Rahi
Seamount Field
Study Area
-120˚
-100˚
20˚
0˚
-20˚
COCOS
PACIFIC
NAZCA
STUDY AREA

Figure 1

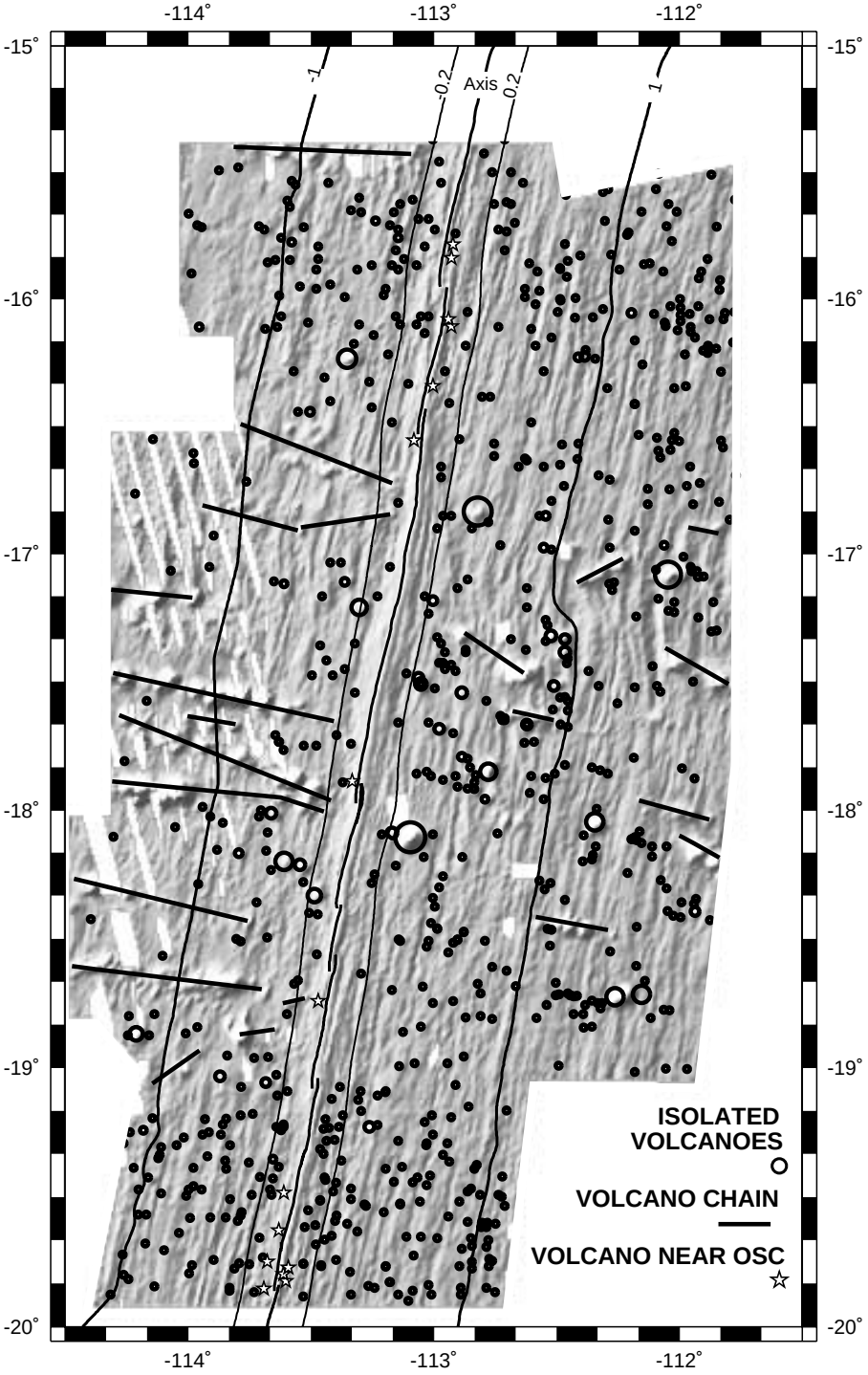
-114˚
-113˚
-112˚
-15˚
-16˚
-17˚
-18˚
-19˚
-20˚
-1
-0.2
Axis
0.2
1
ISOLATED VOLCANOES
VOLCANO CHAIN
VOLCANO NEAR OSC

Figure 2

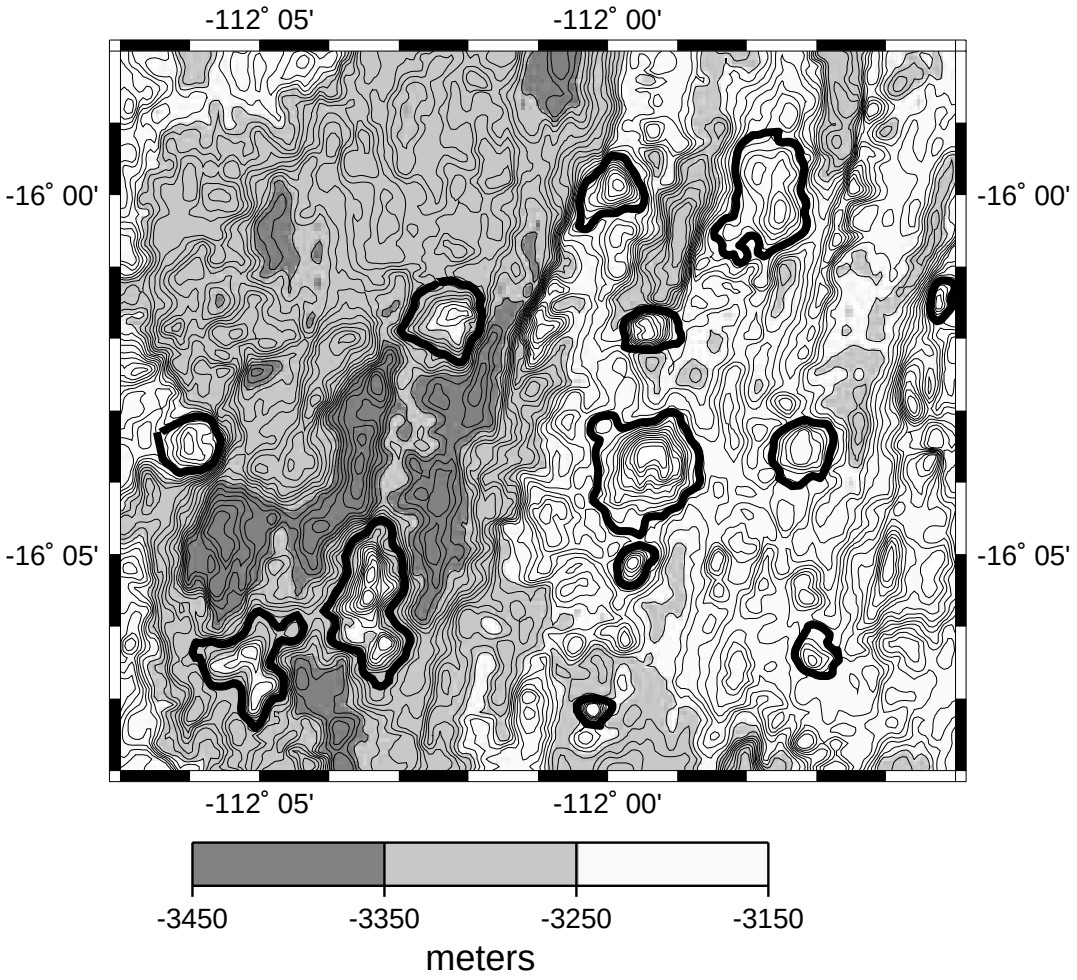

Figure 3a

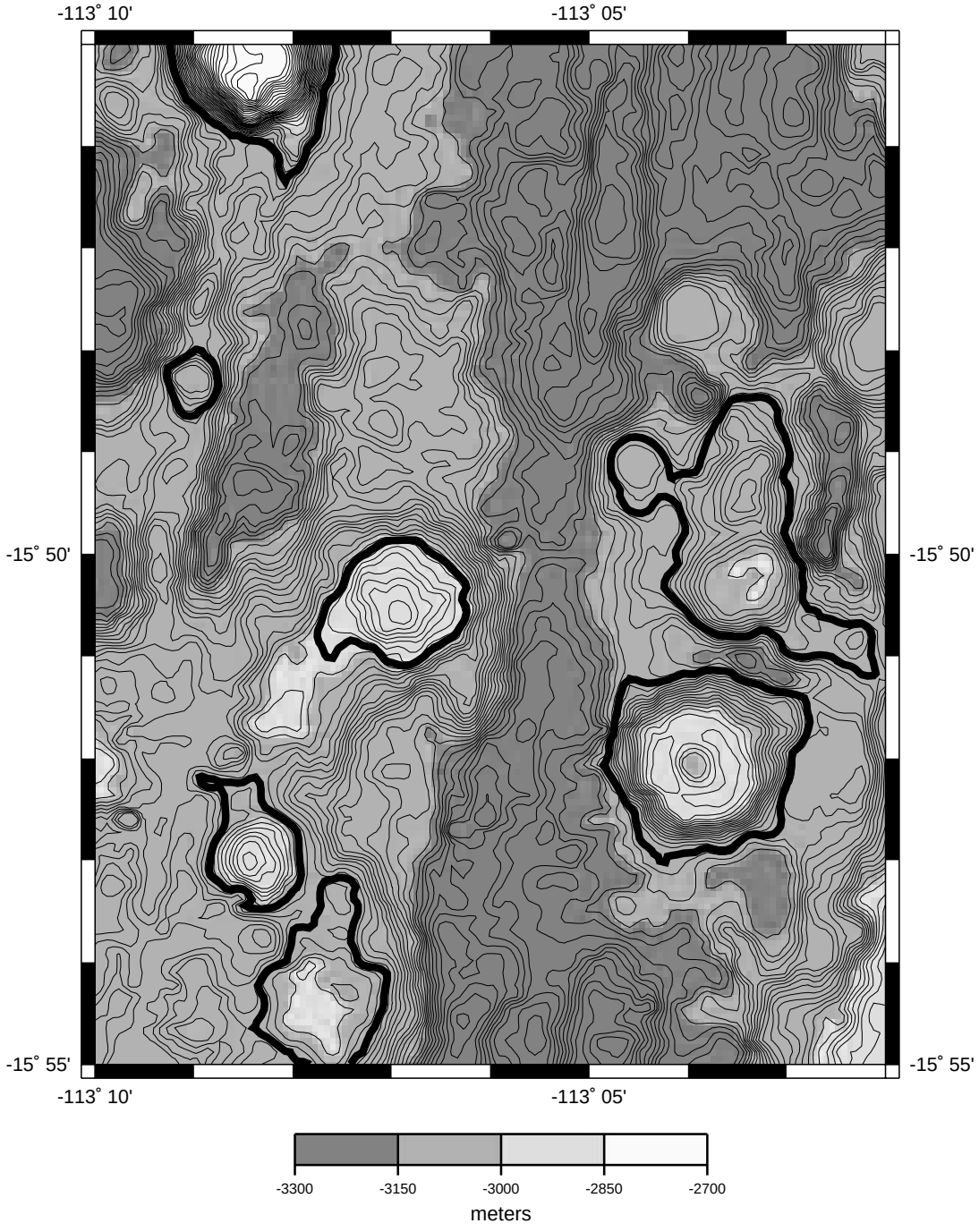

Figure 3b

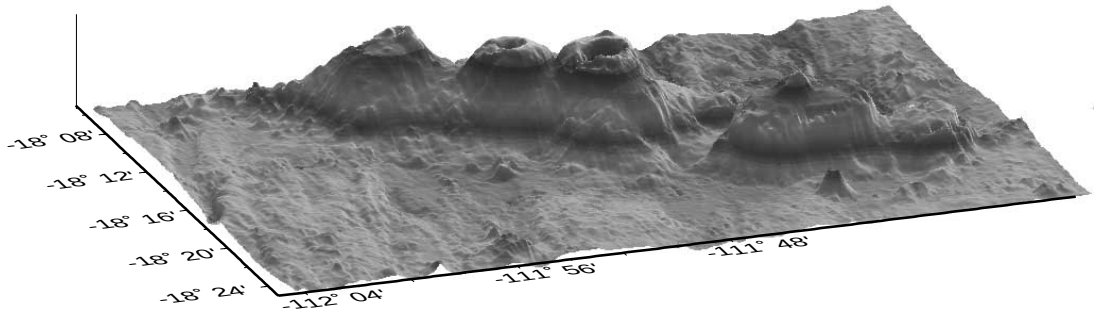

Figure 4

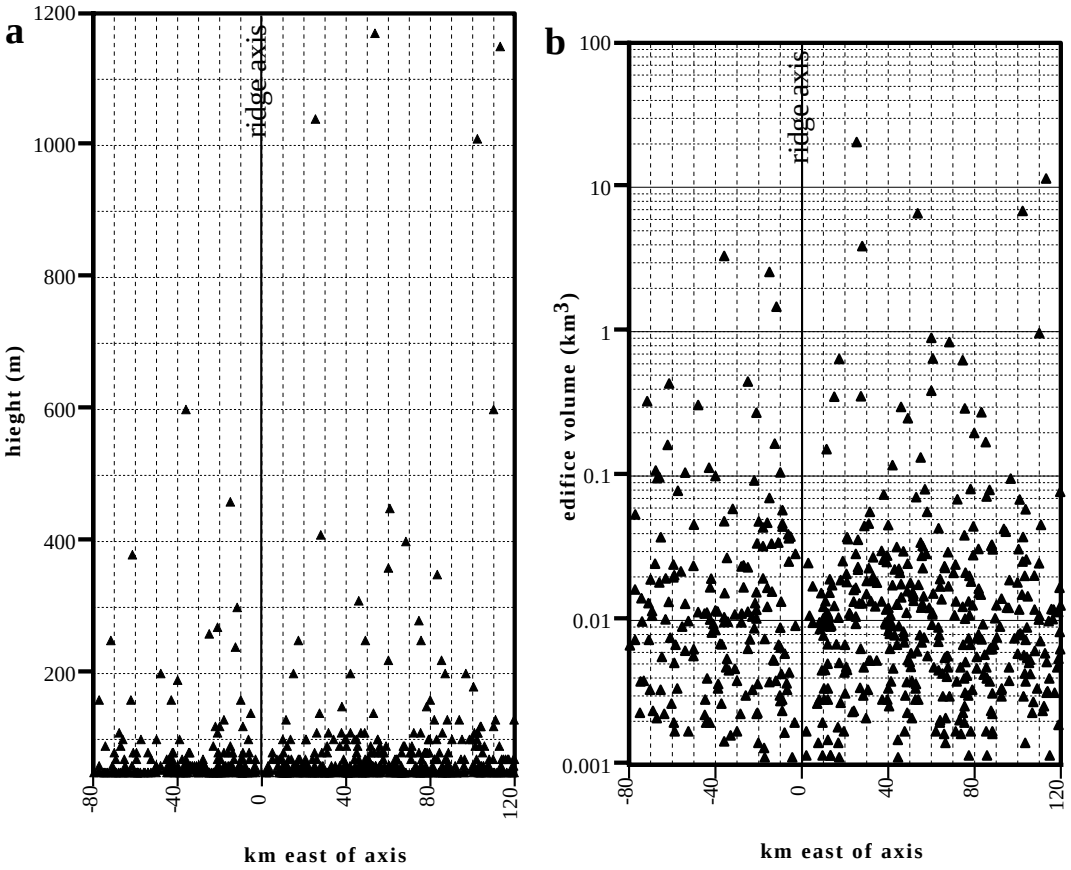

Figure 5

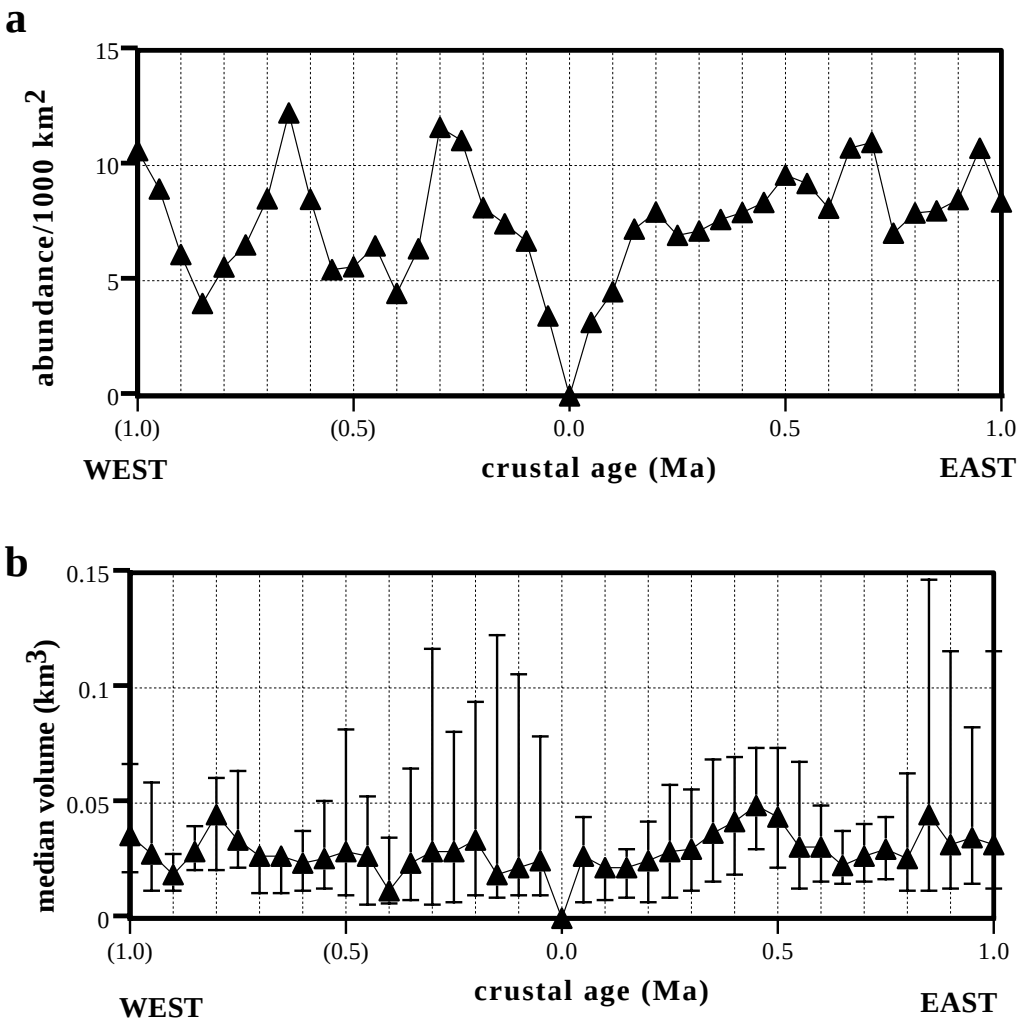
a
abundance/1000 km2
15
10
5
0
(1.0)
(0.5)
0.0
0.5
1.0
WEST
crustal age (Ma)
EAST
b
median volume (km3)
0.15
0.1
0.05
0
(1.0)
(0.5)
0.0
0.5
1.0
WEST
crustal age (Ma)
EAST

Figure 6

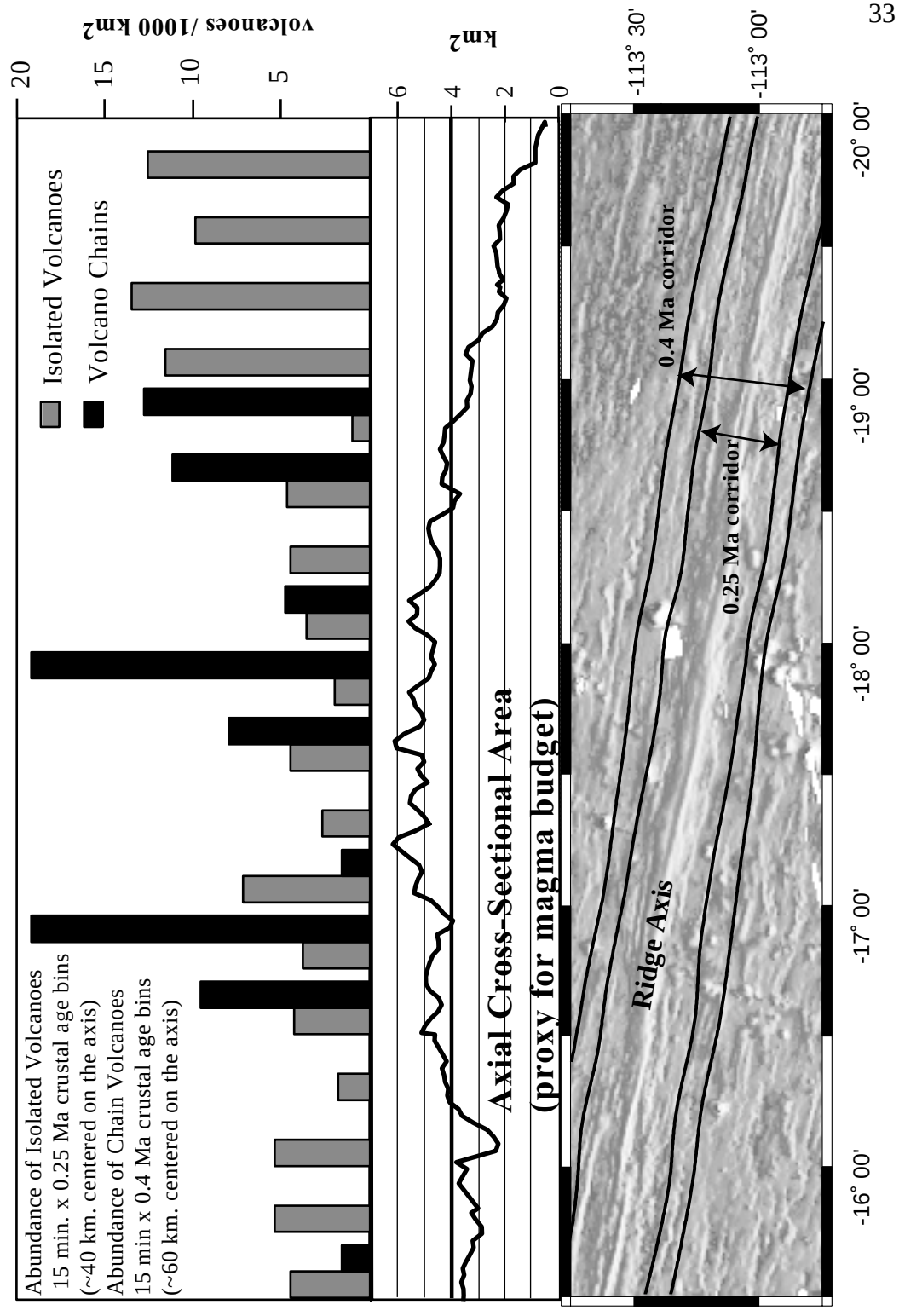
volcanoes /1000 km2
20
15
10
5
km2
6
4
2
0
Isolated Volcanoes
Volcano Chains
Abundance of Isolated Volcanoes
15 min. x 0.25 Ma crustal age bins
(~40 km. centered on the axis)
Abundance of Chain Volcanoes
15 min x 0.4 Ma crustal age bins
(~60 km. centered on the axis)
Axial Cross-Sectional Area
(proxy for magma budget)
-113˚ 30'
-113˚ 00'
-20˚ 00'
-19˚ 00'
-18˚ 00'
-17˚ 00'
-16˚ 00'
0.4 Ma corridor
0.25 Ma corridor
Ridge Axis

Figure 7

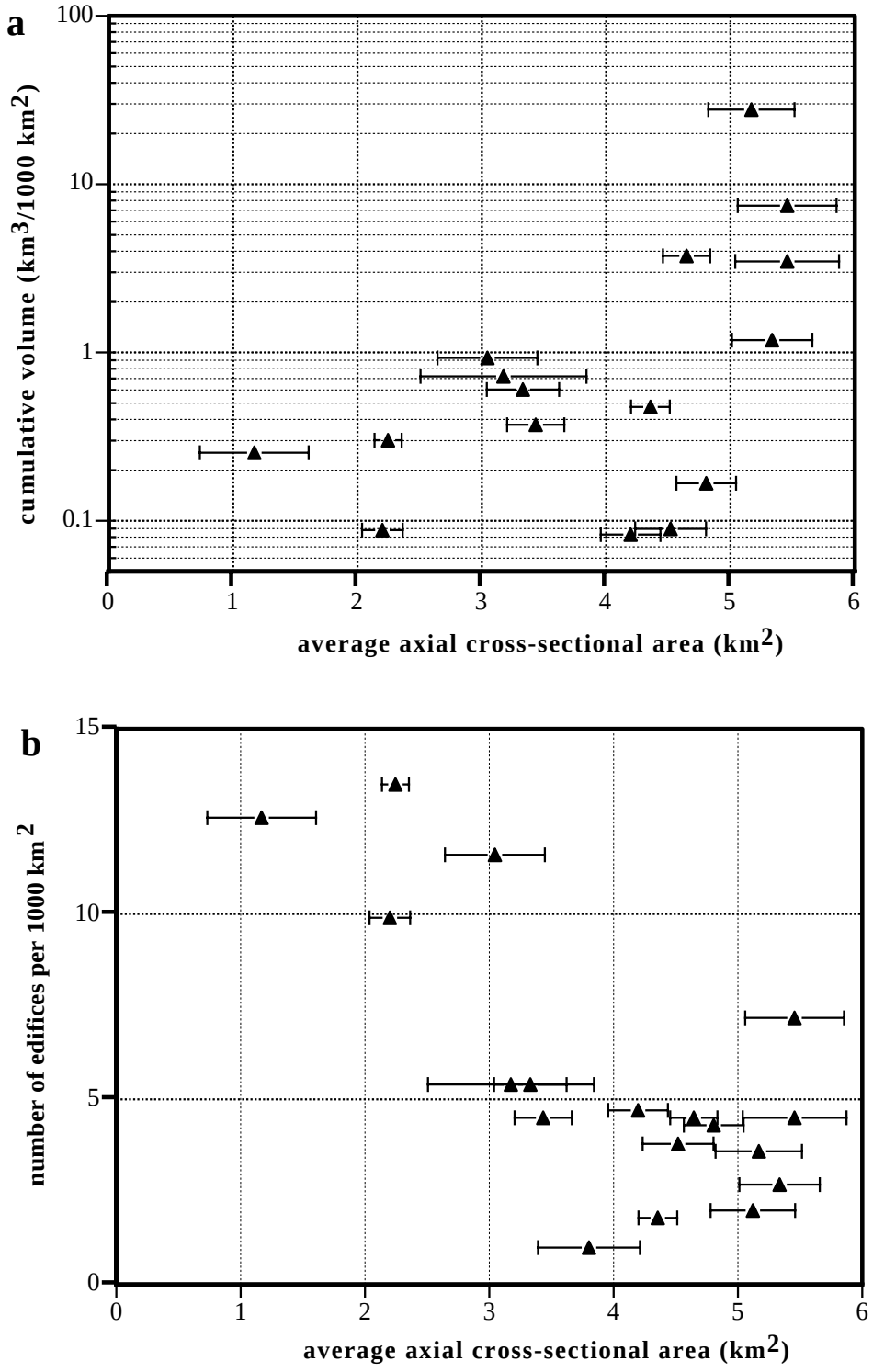
a
100
10
1
0.1
cumulative volume (km3/1000 km2)
0
1
2
3
4
5
6
average axial cross-sectional area (km2)
b
15
10
5
0
number of edifices per 1000 km 2
0
1
2
3
4
5
6
average axial cross-sectional area (km2)

Figure 8

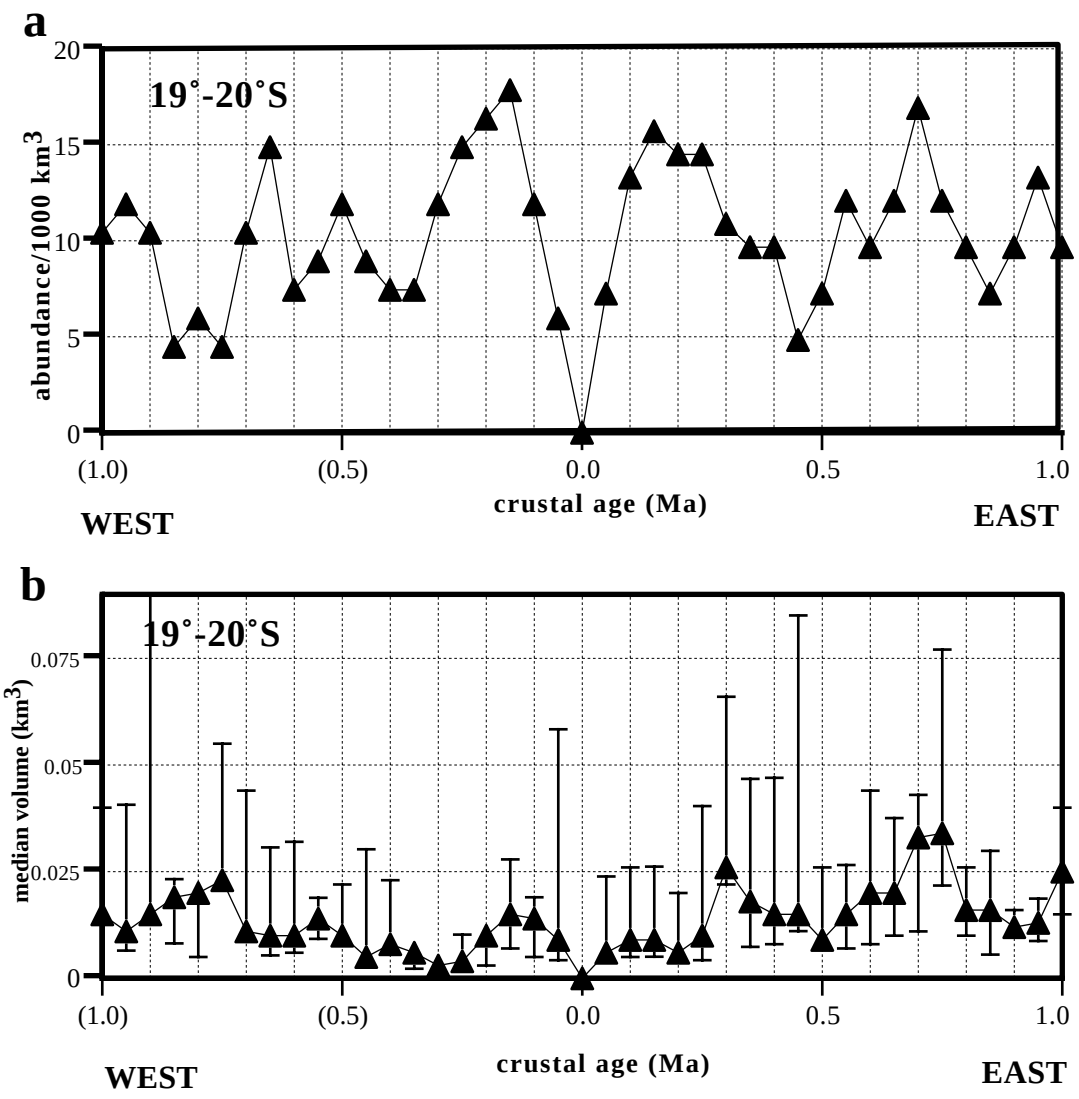
a
19˚-20˚S
abundance/1000 km3
20
15
10
5
0
(1.0)
(0.5)
0.0
0.5
1.0
crustal age (Ma)
WEST
EAST
b
19˚-20˚S
median volume (km3)
0.075
0.05
0.025
0
(1.0)
(0.5)
0.0
0.5
1.0
crustal age (Ma)
WEST
EAST

Figure 9

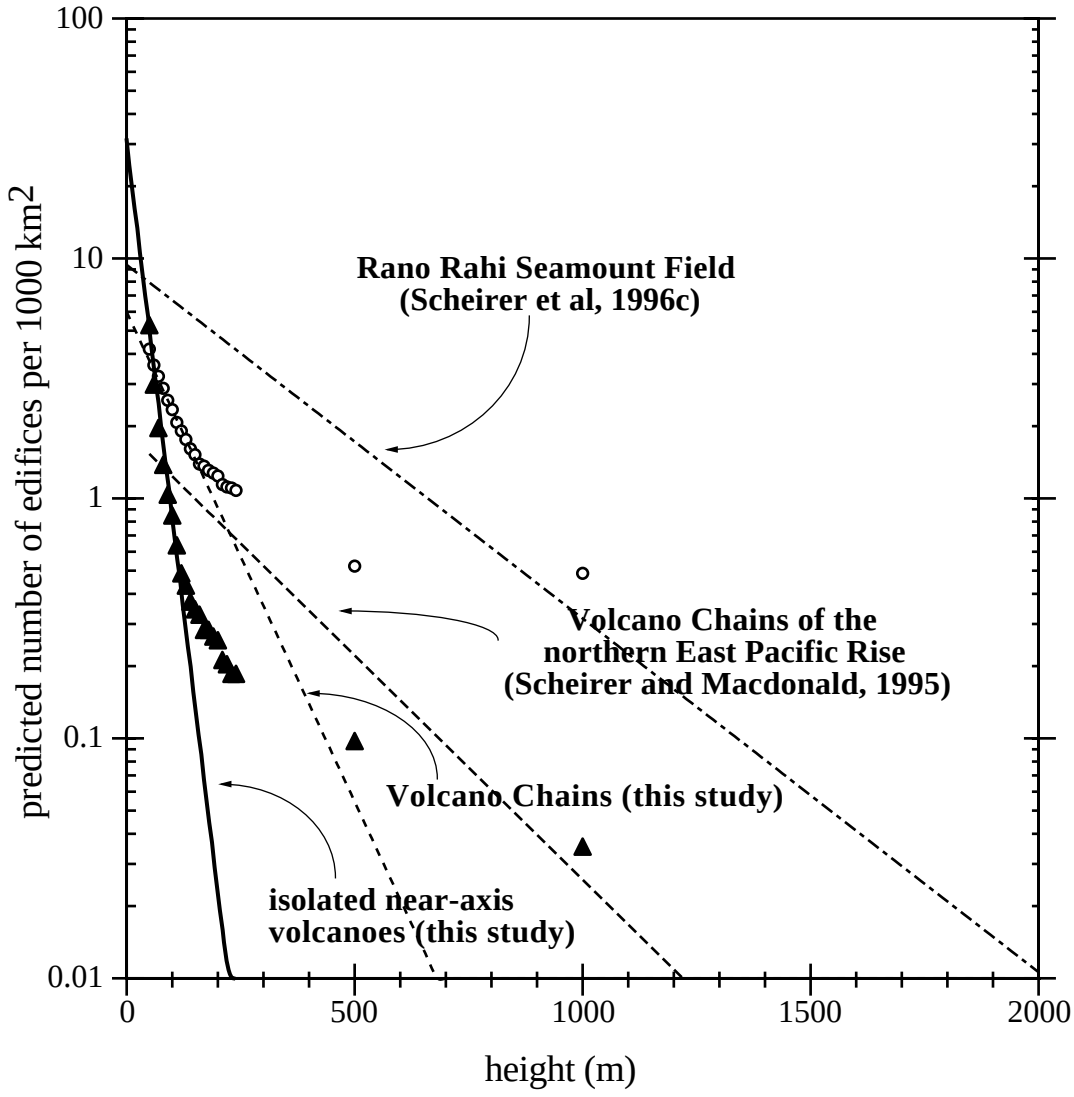
100
10
1
0.1
0.01
predicted number of edifices per 1000 km2
0
500
1000
1500
2000
height (m)
Rano Rahi Seamount Field
(Scheirer et al, 1996c)
Volcano Chains of the
northern East Pacific Rise
(Scheirer and Macdonald, 1995)
Volcano Chains (this study)
isolated near-axis
volcanoes (this study)

Figure 10

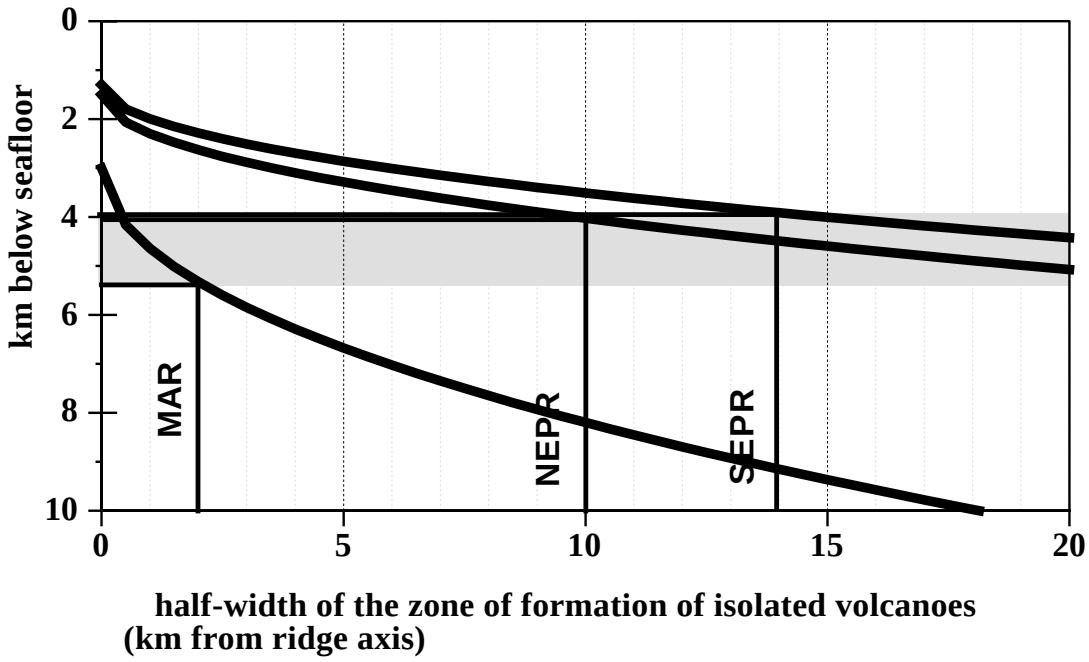
km below seafloor
0
2
4
6
8
10
0
5
10
15
20
MAR
NEPR
SEPR
half-width of the zone of formation of isolated volcanoes
(km from ridge axis)

Figure 11